

# Preliminary qualification of a machine learning-based assessment of the tumor immune infiltrate as a predictor of outcome in patients with hepatocellular carcinoma treated with atezolizumab plus bevacizumab

Bernhard Scheiner, 1,2 Pasquale Lombardi, 1,3 Antonio D'Alessio ,1 Gwangil Kim, 4 Masoud Tafavvoghi, 5 Oleksandr Petrenko ,2,6 Robert D Goldin, 1 Claudia A M Fulgenzi, 1 Aria Torkpour, 1 Lorenz Balcar, 2 Francesco A Mauri, 1 Katharina Pomej, 2 Vera Himmelsbach, 7 Maryam Barsch, 8 Ciro Celsa, 9 Giuseppe Cabibbo, 9 Jaekyung Cheon, 10 Anja Krall, 11 Florian Hucke, 12 Luca Di Tommaso, 13,14 Monica Bernasconi, 14 Lorenza Rimassa, 14,15 Adel Samson, 16 Bernardo Stefanini, 17 Behrang Mozayani, 18 Michael Trauner, 2 Carolin Lackner, 19 Rudolf Stauber, 11 Francesco Vasuri, 20 Fabio Piscaglia, 17,21 Bertram Bengsch, 8 Fabian Finkelmeier, Markus Peck-Radosavljevic, 12 Lill-Tove Rasmussen Busund, 22 Teresa Marafioti, 23 Mohammad Rahbari, 24 Mathias Heikenwalder, 24 Mathias Pinter ,2 Hong Jae Chon, 10 Mehrdad Rakaee ,5,22 David J Pinato 15 1

**To cite:** Scheiner B, Lombardi P, D'Alessio A, *et al.* Preliminary qualification of a machine learning-based assessment of the tumor immune infiltrate as a predictor of outcome in patients with hepatocellular carcinoma treated with atezolizumab plus bevacizumab. *Journal for ImmunoTherapy of Cancer* 2025;**13**:e010975. doi:10.1136/jitc-2024-010975

► Additional supplemental material is published online only. To view, please visit the journal online (https://doi.org/10.1136/iitc-2024-010975).

MR and DJP contributed equally.

Accepted 31 August 2025



© Author(s) (or their employer(s)) 2025. Re-use permitted under CC BY-NC. No commercial re-use. See rights and permissions. Published by BMJ Group.

For numbered affiliations see end of article.

# Correspondence to

Prof. David J Pinato; david.pinato@imperial.ac.uk

Prof Hong Jae Chon; hongjaechon@gmail.com

# **ABSTRACT**

Spontaneously immunogenic hepatocellular carcinoma (HCC), identified by a dense immune cell infiltrate (ICI), responds better to immunotherapy, although no validated biomarker exists to identify these cases. We used machine learning (ML) to quantify ICI from standard H&E-stained tissue and evaluated its correlation with characteristics of the tumor microenvironment (TME) and clinical outcome from atezolizumab plus bevacizumab (A+B). We therefore employed a supervised ML algorithm on 102 pretreatment H&E slides collected from patients treated with A+B. We quantified tumor, stroma and immune cell counts/mm<sup>2</sup> and dichotomized patients into ICI high and ICI low for clinicopathologic analysis. We correlated ICI signature with characteristics of the T-cell infiltrate (CD4+, FOXP3+, CD8+, PD1+) using multiplex immunohistochemistry in 62 resected specimens and evaluated gene expression profiles by bulk RNA sequencing in 44 samples.

All patients treated with A+B were Child-Pugh A and received first-line A+B treatment for Barcelona Clinic Liver Cancer Stage C HCC (n=77, 75.5%) on a background of viral (n=53, 52%) and non-viral (n=49, 48%) liver disease. Median ICl density was 429.9 (IQR: 194.6–666.7) cells/mm². Two-thirds of patients (n=67, 65.7%) had ICl counts≥236/mm², derived as the optimal prognostic cut-off (ICl-high). Baseline characteristics, including disease etiology, liver function, performance status, stage, prior therapy and alpha-fetoprotein (AFP) levels, were comparable between ICl-high versus ICl-low patients. Patients with ICl-high demonstrated a significantly longer

overall survival (OS) compared with ICI-low: 20.9 (95% CI: 13.8 to 27.9) versus 15.3 (95% CI: 6.0 to 24.6 months, p=0.026). Multivariable analyses demonstrated ICI-low status to remain as an independent prognostic parameter (adjusted HR (aHR): 2.02, 95% CI: 1.03 to 3.96) alongside AFP concentration (per 100 ng/mL; aHR 1.00, 95% CI; 1.00 to 1.00). ICI-high tumors were characterized by STC1 underexpression and enrichment in proinflammatory gene expression sets previously associated with response to immunotherapy. The proinflammatory environment identified by ICI status was not exclusively mediated by T-cell phenotype polarization as shown by a lack of correlation between ICI-high status and CD4+, CD4+F0XP3+, CD8+ and CD8+PD1+ T-cell density. In conclusion, we propose a ML-based algorithm to identify proinflamed HCC TMEs bearing a positive correlation with the patient's OS. Digital characterization of the TME should be validated as a tool to improve precision delivery of anticancer immunotherapy.

### INTRODUCTION

Even though the advent of effective combination immunotherapy has improved outcomes in patients with advanced hepatocellular carcinoma (HCC), overall survival (OS) benefit is unevenly distributed across immunotherapy recipients. Additionally, high-grade adverse events may occur in more than half of patients and may lead to death in up



to  $\sim 5\%$ , <sup>12</sup> reducing their therapeutic index. Combination immunotherapy is also associated with significant costs, and the availability of multiple systemic therapy regimens emphasizes the need for better patient selection. <sup>1</sup>

The development of biomarkers that can identify patients who derive greater benefit from treatment remains a major unmet need in HCC.<sup>3</sup> A myriad of bloodbased, tissue-based, imaging-based and clinical parameters have been evaluated for their predictive power,<sup>4</sup> but none has influenced immunotherapy delivery in the clinic.<sup>5</sup> The expanding use of high-throughput technologies in pretreatment tissue samples has led to an immune-based subclassification of the HCC tumor microenvironment (TME) that might identify treatment responders. However, RNA sequencing (RNA-seq) and extended genomic testing are costly, lack reproducibility and are poorly scalable to routine clinical practice.<sup>6</sup>

Accumulating evidence suggests that solid tumors harboring a spontaneously immunogenic, interferon-y rich, proinflamed microenvironment are more likely to respond to immunotherapy. In tumors such as nonsmall cell lung cancer (NSCLC), the status of the TME is efficiently recapitulated by programmed death-ligand 1 (PD-L1) expression status, which serves as a stratification factor for the utilization of programmed cell death protein 1 (PD-1)-targeted monotherapy in a subset of patients.<sup>8</sup> However, the HCC microenvironment is perhaps more complex and more geared towards immune suppression—reasons why perhaps PD-L1 immunohistochemical testing does not predict for outcome from immunotherapy in HCC. 9-11 However, like many other solid tumors, a subset of HCCs is spontaneously immune activated. 9 11 These 'inflamed' subclasses of HCC are associated with upregulation of inflammatory response markers, 11 expression of immune-effector cytokines and a more diverse T-cell repertoire <sup>12</sup>—features that may lead to a better response to immunotherapy.

Machine learning (ML)-based approaches applied to digital pathology may aid in evaluating overall characteristics of the TME and might help to stratify patient outcomes prior to immunotherapy initiation. <sup>13</sup> We recently demonstrated that an ML-based approach was able to accurately detect and quantify immune cell infiltration on routine pretreatment H&E-stained slides derived from patients with NSCLC and found that patients with a dense infiltrate had a better response to immunotherapy. <sup>14</sup>

Building on our experience with other immune-sensitive malignancies, we aimed to develop a ML-based model to quantify tumor, stroma and immune cell counts/mm² in HCC, to derive an optimal prognostic cut-off for clinicopathologic analysis and to correlate the immune cell infiltrate (ICI) signature with the phenotypic characteristics of the T-cell infiltrate (CD4+, FOXP3+, CD8+, PD1+) using multiplex immunohistochemistry. In addition, we compared gene expression profiles in ICI-high/ICI-low tumors to further characterize the respective TMEs and provide an immune-biologic foundation for the proposed ML model.

### **METHODS**

### Study population and material

This study comprised three cohorts (figure 1A). The atezolizumab plus bevacizumab (A+B) cohort included 102 patients who received atezolizumab and bevacizumab as first-line systemic treatment for advanced HCC at eight international centers (Bologna, Graz, Klagenfurt, Leeds, London, Milan, Seoul and Vienna). In this cohort, we collected preimmunotherapy H&E-stained liver tissue slides derived from tumor biopsies (n=67) or liver resection specimens (n=35). The liver resection group included 20 patients in whom systemic treatment was initiated shortly after resection, as complete tumor removal was not possible and/or patients had additional extrahepatic metastases, while in 15 patients systemic treatment was started after tumor recurrence during follow-up. The multiplex immunohistochemistry cohort (mIHC cohort) included 62 patients and the RNA-seg cohort 44 patients who underwent curative resection for HCC. In these two cohorts, we collected tissue slides from formalin-fixed paraffin-embedded resection specimens. H&E-stained slides were digitalized at a resolution of 0.24 or 0.49 microns/pixel. A detailed description of inclusion and exclusion criteria, information on data extraction, processing of mIHC and bulk RNA-seq can be found in the online supplemental file 1.

### ML approach for ICI identification and quantification

The supervised ML algorithm was developed using QuPath (V.0.4.2) and followed the previously described procedure with some modifications. A schematic overview (online supplemental figure 1), a step-by-step guide demonstrating how to apply the method within the QuPath graphical user interface as well as a detailed description of model development, training and quality verification can be found in the online supplemental file 1.

# **Statistics**

Statistical analyses were performed using IBM SPSS Statistics V.26, GraphPad Prism V.8 (GraphPad Software, San Diego, California, USA) and R V.4.3.1 (R Core Team, R Foundation for Statistical Computing, Vienna, Austria).

The optimal prognostic ICI cut-off was derived by the log-rank maximization method as previously described. <sup>16</sup> Univariable and multivariable Cox regression models were used to evaluate prognostic factors for OS and progression-free survival (PFS).

A detailed description of the statistical approach including the approach to RNA-seq data as well as the definition of study endpoints can be found in the online supplemental file 1.

# RESULTS Patients

As outlined in online supplemental figure 2, we screened 138 patients from eight international centres who received

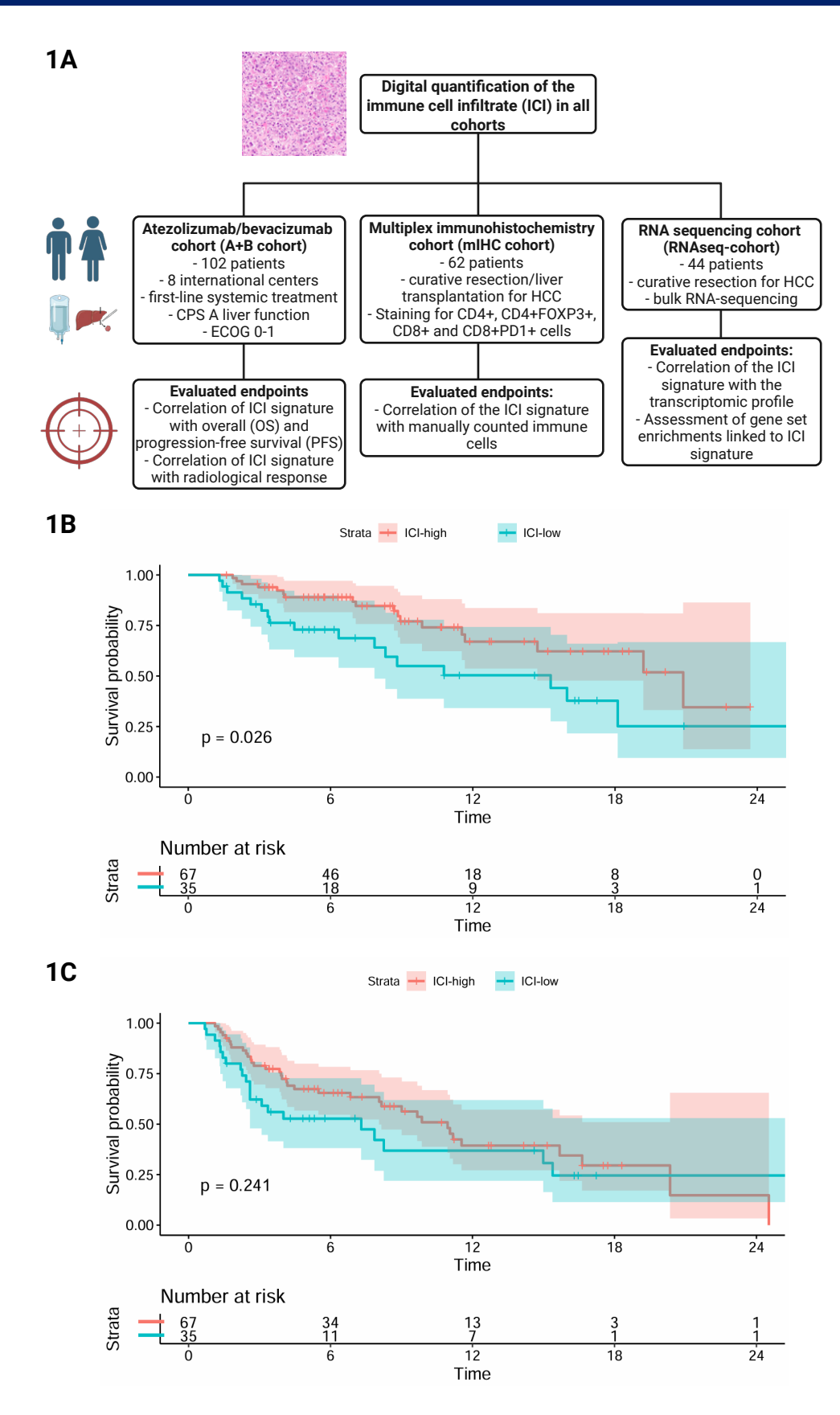


**Figure 1** (A) Study flowchart demonstrating the different study cohorts and evaluated endpoints as well as comparison of (B) overall survival (OS) and (C) progression-free survival (PFS) between patients with ICI high versus ICI low in the *A+B cohort*. CPS, Child-Pugh score; ECOG, Eastern Cooperative Oncology Group; HCC, hepatocellular carcinoma; ICI, immune cell infiltrate cells/mm<sup>2</sup>.

A+B treatment between March 2020 and December 2022, for inclusion into the *A+B cohort*. A total of 36 patients were excluded from the study due to baseline liver function impairment (Child-Pugh Score >7: n=10), the use of non-first-line therapies (n=3) and, in 10 cases, the unavailability of liver tissue for analysis. Consequently, the *A+B cohort* comprised 102 patients.

### Baseline characteristics of the A+B cohort

The majority of patients were men (n=86, 84.3%) with a median age of 68.0 (IQR: 59.7–76.4) years. Two-thirds of patients had underlying liver cirrhosis (n=64, 62.7%) and 75.5% (n=77) had advanced stage HCC (Barcelona Clinic Liver Cancer Stage C (BCLC-C)). Median pretreatment ICI Score was 429.9 (194.6–666.7) cells/mm<sup>2</sup>. Further patient characteristics are outlined in table 1.

# Prognostic importance of ML-derived assessment of the TME

To evaluate the prognostic importance of the ML-derived assessment of the TME, we performed restricted cubic spline analysis to quantify the effect of ICI counts (cells/mm<sup>2</sup>) on OS. We found that patients with lower ICI counts had a significantly increased risk for mortality (online supplemental figure 3A). For clinical application, we next performed a maximally selected rank statisticsbased assessment of the optimal ICI cut-off for OS prediction. This cut-point was derived at 235.02 and rounded to 236 cells/mm<sup>2</sup> (online supplemental figure 3B). Baseline characteristics were comparable between 35 patients with ICI-low (<236/mm<sup>2</sup>; median tumor infiltrating lymphocyte (TIL) counts: 163.1, IOR: 120.0-197.3) and 67 patients with ICI-high (≥236/mm<sup>2</sup>; median TIL counts: 600.3, IOR: 242.6-2258.3, table 1). Importantly, patients with ICI-high had a significantly better median OS as compared with ICI-low (ICI-high: 20.9, 95% CI: 13.8 to 27.9 months versus ICI-low: 15.3, 95% CI: 6.0 to 24.6 months; p=0.026; figure 1B), while no PFS benefit was observed (ICI-high: 10.9, 95% CI: 8.7 to 13.2 months versus ICI-low: 7.3, 95% CI: 1.4 to 13.2 months; p=0.241, figure 1C). Radiological response (ORR: ICI-high: n=20 (29.9%) versus ICI-low: n=8 (22.9%); p=0.452; disease control rate: ICI-high: n=53 (79.1%) versus ICI-low: n=22 (62.9%); p=0.077) was not statistically significantly different (table 1).

Finally, we performed univariable and multivariable analyses of factors associated with OS. Interestingly, only AFP levels (per 100ng/mL: adjusted HR (aHR): 1.00, 95% CI: 1.00 to 1.00; p=0.038) and ICI-high status (aHR: 2.02, 95% CI: 1.03 to 3.96; p=0.040) were independently associated with OS (table 2).

# Comparison of the density of manually counted immune cells within the ICI-high and ICI-low groups in the mIHC cohort

The *mIHC cohort* included 62 patients who underwent liver resection or transplantation for early (BCLC A: n=53, 85.5%) or intermediate stage (BCLC B: n=9, 14.5%) HCC between April 2004 and February 2019. The majority of patients were men (79.3%) with a

median age of 55.5 (IQR: 50.7–61.0) years. Detailed baseline patient characteristics are displayed in online supplemental table 1.

Median ICI counts in this cohort were 432.2 (IQR: 284.2–596.3) cells/mm², and while 49 patients (79.0%) were attributed to the ICI-high group, 13 patients were allocated to the ICI-low group. As the ICI evaluation was performed on whole slide scans, the manually counted immune cell infiltrate (performed separately for non-tumoral, peritumoral and intratumoral areas) was averaged, resulting in a median of 366.2 (IQR: 231.5–566.4) CD4+ cells/mm², 33.4 (IQR: 10.9–61.5) CD4+FOXP3+ cells/mm², 296.8 (IQR: 210.0–462.9) CD8+ cells/mm² and 50.6 (IQR: 13.6–84.4) CD8+PD1+ cells/mm².

Online supplemental figure 4 demonstrates median immune cell counts in patients with ICI high versus ICI low, and online supplemental figure 5 shows two representative sections from mIHC slides at two different magnifications. While CD4+, CD4+FOXP3+ and CD8+PD1+ T-cell counts were comparable between patients with high versus low ICI counts, we observed a trend towards higher CD8+ T-cell counts in the ICI-high group (p=0.074).

### **Transcriptomic features of ICI-high patients**

Finally, transcriptomic profiling and weighted gene coexpression network analysis were performed on 44 patients who underwent resection or transplantation for HCC (figure 2A, online supplemental file 1). The primary objective was to further characterize the TME as reflected by the presence and density of the ICI and to provide a technical validation of the ICI score. Therefore, transcriptomic profiles were compared between two extreme groups: patients with ICI scores above the 66th and below the 33rd percentile. Overall, 1507 differentially expressed genes were detected (figure 2B, online supplemental figure 9). Even though separation was not perfect, principal component 1 (PC1) and PC3 allowed for the best separation (online supplemental figure 8). The genes and gene sets contributing to PC1 and PC3 are outlined in online supplemental figure 8. While pathways associated with inflammation (eg, those associated with allograft rejection, inflammatory response, TNF $\alpha$ -signaling via NF $\kappa$ B, interferon- $\gamma$ , etc) were significantly overexpressed in ICI-high patients, pathways associated with metabolite metabolism (eg, fatty acid metabolism, bile acid metabolism, etc) were overexpressed in ICI-low patients (figure 2C, online supplemental figure 9A). Functional pathway enrichment analysis visually confirming these results is shown in online supplemental figure 10. Detailed results, including overlaps between significant gene sets and the expression direction of their key genes, are demonstrated in online supplemental figure 9B,C. Finally, we performed gene coexpression analysis and linked modules of highly coexpressed genes to patient



**Table 1** Patient characteristics and summary of survival outcomes and radiological response for patients with ICI high (≥236 cells/mm²) versus ICI low (<236 cells/mm²)

	All patients (n=102)	ICI low (n=35)	ICI high (n=67)	P value	
Age (years), median (IQR)	68.0 (59.7–76.4)	69.4 (60.5–76.0)	67.0 (59.6–77.3)	0.794	
Sex					
Male, n (%)	86 (84.3%)	29 (82.9%)	57 (85.1%)	0.770	
Cirrhosis, n (%)	64 (62.7%)	18 (51.4%)	46 (68.7%)	0.088	
Etiology of liver disease					
HBV, n (%)	34 (33.3%)	12 (34.3%)	22 (32.8%)	0.883	
HCV, n (%)	19 (18.6%)	9 (25.7%)	10 (14.9%)	0.184	
Alcohol, n (%)	22 (21.6%)	4 (11.4%)	18 (26.9%)	0.072	
NAFLD/NASH, n (%)	21 (20.6%)	6 (17.1%)	15 (22.4%)	0.534	
Other, n (%)	9 (8.8%)	5 (14.3%)	4 (6.0%)	0.268	
Child-Pugh Score					
5 points, n (%)	74 (72.5%)	25 (71.4%)	49 (73.1%)	0.855	
6 points, n (%)	28 (27.5%)	10 (28.6%)	18 (26.9%)		
ECOG PS					
0, n (%)	50 (49.0%)	19 (54.3%)	31 (46.3%)	0.442	
1, n (%)	52 (51.0%)	16 (45.7%)	36 (53.7%)		
BCLC stage					
A, n (%)	5 (4.9%)	3 (8.6%)	2 (3.0%)	0.441	
B, n (%)	20 (19.6%)	6 (17.1%)	14 (20.9%)		
C, n (%)	77 (75.5%)	26 (74.3%)	51 (76.1%)		
Previous treatments					
Surgery, n (%)	41 (41.0%)	12 (35.3%)	29 (43.9%)	0.405	
RFA/MWA, n (%)	10 (10.1%)	5 (14.7%)	5 (7.7%)	0.271	
TACE, n (%)	34 (34.0%)	8 (23.5%)	26 (39.4%)	0.113	
TARE, n (%)	3 (3.0%)	2 (5.9%)	1 (1.5%)	0.231	
EBRT, n (%)	13 (13.4%)	4 (12.1%)	9 (14.1%)	0.790	
AFP (ng/mL), median (IQR)	29.3 (4.8–642.0)	29.0 (4.0–2397.0)	29.6 (5.4–642.0)	0.619	
Best overall response					
CR/PR	28 (27.5%)	8 (22.9%)	20 (29.9%)	0.209	
SD	47 (46.1%)	14 (40.0%)	33 (49.3%)		
PD/NE	27 (26.5%)	13 (37.1%)	14 (20.9%)		
ORR (CR+PR)*	28 (27.5%)	8 (22.9%)	20 (29.9%)	0.452	
DCR (CR+PR+SD)†	75 (73.5%)	22 (62.9%)	53 (79.1%)	0.077	

<sup>\*</sup>Patients who were not evaluable were considered as not having an objective response.

AFP, alpha-fetoprotein; BCLC, Barcelona Clinic Liver Cancer; CR, complete response; DCR, disease control rate; EBRT, external beam radiation therapy; ECOG PS, Eastern Cooperative Oncology Group Performance Status; HBV, hepatitis B virus; HCV, hepatitis C virus; ICI, immune cell infiltrate; MWA, microwave ablation; NAFLD, non-alcoholic fatty liver disease; NASH, non-alcoholic steatohepatitis; N/E, not evaluable; ORR, objective response rate; PD, progressive disease; PR, partial response; RFA, radiofrequency ablation; SD, stable disease; TACE, transarterial chemoembolization; TARE, transarterial radioembolization.

metadata (online supplemental figure 11). Module 4 had the highest correlation with ICI level, and among the most significant genes, STC1 and EPS8L3 were highly enriched in ICI-low patients. Previous reports have shown the potential of these genes in conferring

resistance to immunotherapy.<sup>17</sup> A more detailed description of the results of our transcriptomic analyses can be found in the online supplemental file 1.

<sup>†</sup>Patients who were not evaluable were considered as not having a controlled disease.

**Table 2** Univariable and multivariable analyses of prognostic factors for overall survival in patients with hepatocellular carcinoma treated with atezolizumab and bevacizumab

		Univariable		Multivariable	Multivariable	
		HR (95% CI)	P value	aHR (95% CI)	P value	
Age	Per year	1.01 (0.98 to 1.04)	0.613	_		
Sex	Male versus female	0.74 (0.29 to 1.92)	0.540	-		
Cirrhosis	Present versus absent	1.16 (0.59 to 2.27)	0.667	-		
ECOG PS	1 versus 0	1.46 (0.73 to 2.91)	0.290	_		
Portal vein thrombosis	Present versus absent	0.68 (0.34 to 1.36)	0.279			
Extrahepatic metastases	Present versus absent	1.09 (0.56 to 2.12)	0.798	-		
BCLC	C versus A/B	1.00 (0.45 to 2.22)	0.992	-		
Alpha-fetoprotein	per 100 ng/mL	1.00 (1.00 to 1.00)	0.018	1.00 (1.00 to 1.00)	0.038	
ICI	ICI low (<236/ mm²) versus ICI high (≥236/ mm²)	2.09 (1.08 to 4.07)	0.029	2.02 (1.03 to 3.96)	0.040	

Values in bold indicate results with P value <0.05.

aHR, adjusted HR; BCLC, Barcelona Clinic Liver Cancer; ECOG PS, Eastern Cooperative Oncology Group Performance Status; ICI, immune cell infiltrate.

### DISCUSSION

Evidence of pre-existing immunogenicity within the TME has emerged as a tumor-agnostic trait correlating with improved outcomes from immune-checkpoint inhibitor-based therapies. 18 While certain surrogates of spontaneous immunogenicity such as PD-L1 status by IHC are consolidated stratifying biomarkers in other cancer types such as NSCLC, 8 no easily scalable biomarkers exist to classify patients with HCC based on the contexture of their TME. ML quantitative methods applied to digital pathology can potentially derive information on the immunogenic polarisation of the TME. Evidence for the clinical utility of ML models derived from routinely available pretreatment H&E-stained slides has emerged quite strongly in NSCLC, where ML outperforms routinely employed predictive biomarkers of benefit to immunotherapy such as PD-L1 status or tumor mutational burden.1

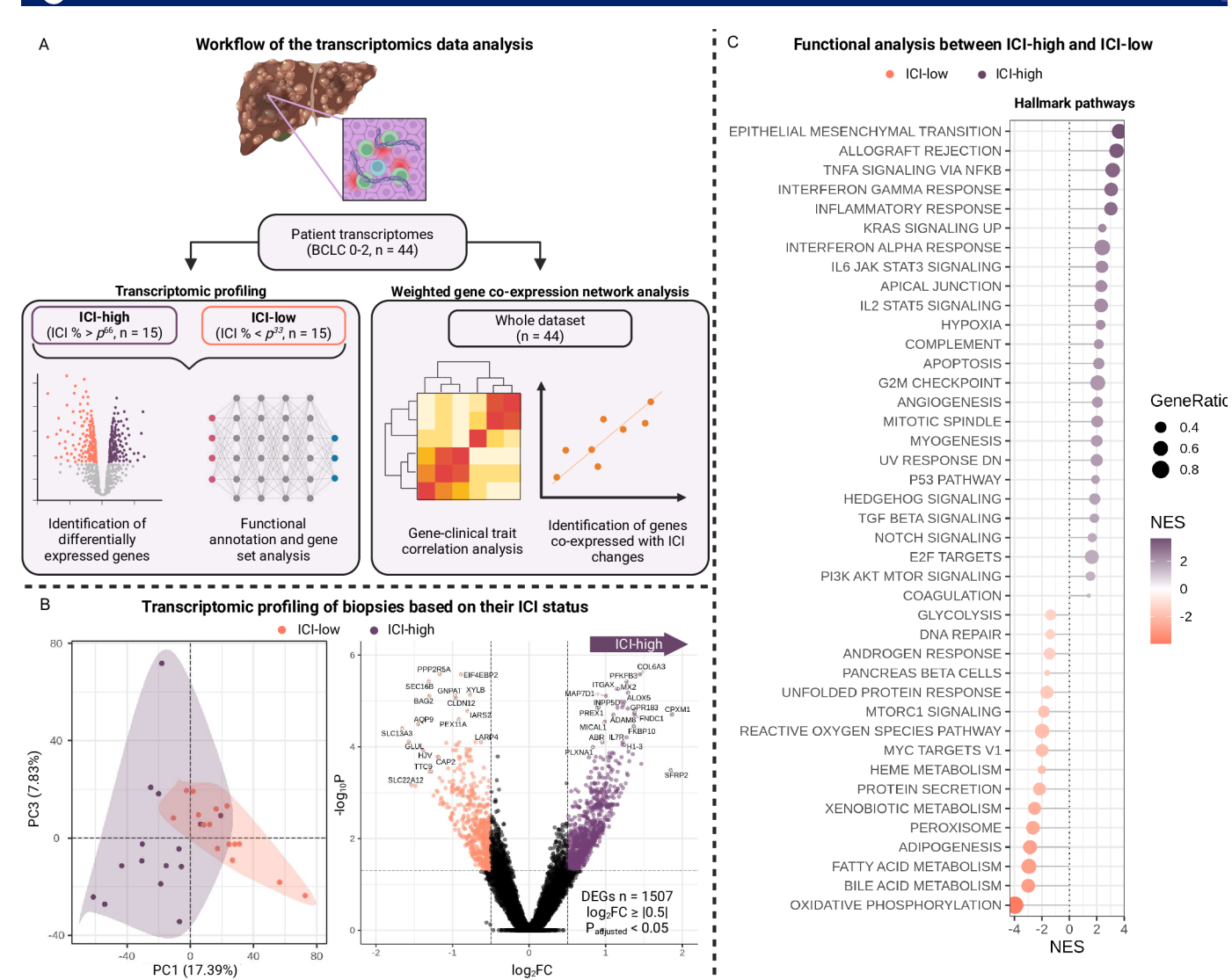
In this preliminary study, we applied a similar methodology on H&E-stained slides derived from patients with HCC prior to treatment with A+B and evaluated the capacity of our model to predict clinical outcomes.

We found that our digital pathology model was able to identify a group of ICI-high specimens uniquely characterized by a denser immune cell infiltrate prior to treatment, a finding that was associated with a more favorable OS—the 'gold standard' endpoint in cancer drug development for advanced HCC. <sup>19</sup> Interestingly, ICI-high status was not associated with any of the common clinicopathologic factors for HCC, was equally distributed across aetiology and remained as a

significant prognostic factor in multivariable models, suggesting its truly independent predictive value for OS in our patient population. Although a higher proportion of responders was observed in the ICI-high group compared with the ICI-low group, the result did not attain statistical significance, and our algorithm seems to rather correlate with patients who are less likely to exhibit inherent resistance to this treatment. Whilst therapeutic benefit is generally higher in patients who achieve a response to immunotherapy, accumulating evidence suggests this is not a prerequisite for long-term survivorship.<sup>20</sup> Furthermore, in the specific case of A+B, the anti-VEGF component of the regimen may further complicate the prediction of response, given the anti-VEGF-driven normalization of the tumor vasculature may lead to response irrespective of the baseline immune cell status of the patient.<sup>21</sup>

To further understand the immunobiological basis of the ICI-based signature identified, we interrogated a separate series of archival resection and transplantation specimens to identify cardinal T-cell populations involved in checkpoint inhibitor resistance in HCC with targeted multiplex-IHC<sup>6</sup> and used RNA-seq to compare and contrast tissue transcriptomics across ICI-high versus ICI-low specimens.

ICI was defined as mononuclear immune cells, including both lymphocytes and plasma cells. <sup>14</sup> <sup>22</sup> To determine which subsets are detected by the ML model, we examined CD8, CD4, Treg and immune-exhausted CD8+PD-1+ T cells. Manual assessment of



(A) Scheme of the RNA sequencing data analysis. The analysis strategy included transcriptomic profiling to identify genes and pathways differentially expressed between patients with ICI-high and ICI-low (left). The second part (right) used weighted gene coexpression network analysis to identify genes whose expression changes with ICI abundance. (B) Principal component analysis and differentially expressed genes between ICI-high and ICI-low. The genes with the highest significance and Log2 fold changes are labeled. (C) Gene set analysis (GO:BP) of differentially expressed genes between ICI-high and ICI-low. AKT, protein kinase B; BCLC, Barcelona Clinic Liver Cancer; DEGs, differentially expressed genes; E2F, early region 2 binding factor; ICI, immune cell infiltrate cells/mm<sup>2</sup>; log<sub>o</sub>FC, log fold change; MTOR, mechanistic target of rapamycin; MYC, MYC proto-oncogene; NES, Normalized Enrichment Score; NFKB, nuclear factor kappa-light-chain enhancer of activated B cells; PC, principal component; PI3K, phosphatidylinositol 3-kinase; TGF BETA, transforming growth factor beta; TNFA, tumor necrosis factor alpha; UV RESPONSE DN, collection of genes downregulated following exposure to ultraviolet radiation.

CD8/mm<sup>2</sup> showed a trend association with ML-based ICI/mm<sup>2</sup> counts, highlighting how T-cell polarisation contributes to ICI but does not exclusively nor univocally define it. Functional analysis of differentially regulated transcripts identified gene sets (GSEA hallmark and Gene Ontology) associated with epithelial to mesenchymal transition and inflammation, identifying candidates such as IFN-γ, IFN-α, TNF-α and interleukin 6 as key functional components of the ICIhigh signature. Interestingly, in coexpression analysis, we found that STC1 and EPS8L3 were highly enriched in ICI-low patients. While tumor STC1 inhibits phagocytosis, thereby contributing to HCC immune evasion

and immunotherapy resistance, 17 EPS8L3 was associated with cell proliferation and migration as well as a poor prognosis.<sup>23</sup>

Even though our study lacks a direct comparison with spatial transcriptomics data, the improved OS seen in ICIhigh tumors, which harbour a uniquely immunogenic and proinflamed milieu, is provocative in suggesting how artificial intelligence (AI)-based models may recapitulate functionally relevant polarization of the TME in the clinic.

Recently, Zeng et al demonstrated that an AI-based algorithm was able to predict the expression of a gene signature previously associated with response to A+B treatment (ie, the AB response signature, (ABRS)) in 122 patients. They also observed that patients with ABRS-high tumors had a significantly better PFS. <sup>24</sup> The authors further investigated their AI prediction using spatial transcriptomics and found a good agreement between the actual gene signature and the AI prediction. <sup>24</sup>

Our study represents the next step in the advancement of quantitative AI-based digital pathology for outcome prediction in HCC. The inclusion of two additional cohorts to elucidate the underlying mechanisms, coupled with the global initiative including several European and Asian centres represent a significant strength of our study. Nevertheless, our study acknowledges several limitations. First, the inclusion of a single, retrospective treatment cohort warrants external validation in subsequent prospective studies before our biomarker can be considered for clinical application.

In addition, to fully differentiate prognostic versus predictive value, including a separate cohort of patients treated with other therapies would importantly clarify whether the improved survival of ICIhigh patients can truly and exclusively be attributed to treatment exposure. Further studies are required to assess whether our ICI-high signature is associated with survival or radiological response in patients treated with different regimens (eg, IO-IO combinations). Ideally, such comparisons should be conducted on prospectively collected trial datasets to avoid treatment allocation bias. Third, our preliminary model considers the immune infiltration status of the totality of the sample without differentiation across regions of interest (tumor and stroma). The limitation of the manual mIHC evaluation to specific regions of interest may explain the lack of correlation with our ML-derived score as the ICI infiltrate may not be homogenous across all regions. To overcome this issue, the use of deep learning models that automatically identify different tumor regions and categorize patients into inflamed versus immune-excluded and immune-desert phenotypes might further refine TME characterization and outcome prediction in HCC.<sup>25</sup> Further studies using an ML-based assessment of the TME should ideally perform all assessments in the same cohort. In our study, we had to perform translational analyses in cohorts of patients with earlier tumor stages (eg, those undergoing resection) as we were unable to recruit a sufficient number of unstained slides in the A+B cohort due to material transfer limitations. Additionally, further studies to evaluate the impact of both tissue acquisition method (surgical resection versus biopsy) and the time interval between tissue collection and the initiation of immunotherapy on the results are strongly encouraged. Finally, future studies should also aim to delineate functional phenotypes of infiltrating T cells using advanced technologies such as singlecell RNA-seq or high-plex IF as different subsets may differentially influence immunotherapy outcomes.<sup>26</sup>

In conclusion, we have developed a preliminary ML model capable of identifying immune cell-enriched tumors with distinctive proinflammatory characteristics within the corresponding TME. Patients classified as ICI high in our retrospective cohort exhibited a superior OS following A+B treatment, lending detection of ICI-high status as a potential biomarker of improved outcome warranting validation with more sophisticated models also considering different regions of interest in prospective studies. Future studies should also focus on the correlation with A+B response signatures as well as further elucidate the role of key genes such as STC1 for response to immunotherapy.

### **Author affiliations**

<sup>1</sup>Imperial College London Department of Surgery and Cancer, London, UK <sup>2</sup>Division of Gastroenterology and Hepatology, Department of Medicine III, Medical University of Vienna, Vienna, Austria

<sup>3</sup>Phase 1 Unit, Fondazione Policlinico Universitario A. Gemelli, IRCCS, Università Cattolica del Sacro Cuore, Rome, Italy

<sup>4</sup>Department of Pathology, CHA Bundang Medical Center, CHA University, Seongnam, Republic of Korea

Department of Cancer Genetics, Oslo University Hospital, Oslo, Norway
 Ukrainian Institute for Systems Biology and Medicine, 04119 Kyiv, Ukraine
 Department of Gastroenterology and Hepatology, University Hospital Frankfurt, Frankfurt, Germany

Department of Internal Medicine II, Medical Center - University of Freiburg, Freiburg, Germany

<sup>9</sup>Gastroenterology and Hepatology Unit, Department of Health Promotion, Mother & Child Care, Internal Medicine & Medical Specialties, University of Palermo, Palermo, Italy

<sup>10</sup>Medical Oncology, Department of Internal Medicine, CHA Bundang Medical Center, CHA University School of Medicine, Seongnam, South Korea

<sup>11</sup>Department of Internal Medicine, Division of Gastroenterology and Hepatology, Medical University of Graz, Graz, Steiermark, Austria

<sup>12</sup>Internal Medicine and Gastroenterology (IMuG), Including Centralized Emergency Service (ZAE), Klinikum Klagenfurt am Wörthersee, Klagenfurt, Kärnten, Austria
<sup>13</sup>Department of Pathology, IRCCS Humanitas Research Hospital, Rozzano, Italy

<sup>14</sup>Department of Biomedical Sciences, Humanitas University, Pieve Emanuele, Milan, Italy

<sup>15</sup>Medical Oncology and Hematology Unit, Humanitas Cancer Center, IRCCS Humanitas Research Hospital, Rozzano, Milan, Italy

<sup>16</sup>Leeds Institute of Medical Research at St James's (LIMR), School of Medicine, Faculty of Medicine and Health, University of Leeds, St James's University Hospita, Leeds, UK

<sup>17</sup>Department of Medical and Surgical Sciences, Bologna University, 40138 Bologna, Italy

<sup>18</sup>Department of Pathology, Medical University of Vienna, Vienna, Austria

<sup>19</sup>Diagnostic and Research Institute of Pathology, Medical University of Graz, Graz, Austria

<sup>20</sup>Pathology Unit, IRCCS - Azienda Ospedaliero-Universitaria di Bologna, 40138 Bologna, Italy

<sup>21</sup>Division of Internal Medicine, Hepatobiliary and Immunoallergic Diseases, IRCCS Azienda Ospedaliero-Universitaria di Bologna, 40138 Bologna, Italy

<sup>22</sup>Department of Clinical Pathology, University Hospital of North Norway, Tromso, Norway

<sup>23</sup>Department of Histopathology, University College London Hospital, London, UK
<sup>24</sup>Division of Chronic Inflammation and Cancer, German Cancer Research Center (DKFZ), Heidelberg, Germany

**Contributors** Concept and design: BSc, AD'A, MRak and DJP. Acquisition and analysis of data: All authors. Writing of the manuscript: BSc, MRak, OP and DJP. All authors have approved the final version. DJP acts as a guarantor of this article.

**Funding** This study was supported by a grant from the Imperial College Healthcare 'Cancer Clinical Trials Committee' (BSc, DJP), a UKRI Impact Acceleration Award, Health Society 2023 (DJP), a Cancer Research UK Imperial Centre PhD studentship



(AT, DJP; reference SEBCATP-2024/100009), an ESMO Fellowship (PL, DJP) and a National Research Foundation of Korea (NRF) grant funded by the Korean government (MSIT) (NRF-2023R1A2C2004339). Furthermore, the research leading to these results has received funding from AIRC under IG 2020—ID. 25087 project—PI LDT.

**Competing interests** BSc received grant support from AstraZeneca and Eisai, speaker honoraria from Eisai and AstraZeneca, as well as travel support from AbbVie, AstraZeneca, Ipsen and Gilead and Roche. PL, GK, MTa, OP, RDG, CAMF, AT, LB, FAM, KP, VH, MBa, CC, GC, JC, AK, AS, BSt, FV, FP, BB, FF, L-TRB, TM, MRah and MH have nothing to disclose. AD'A received educational support for congress attendance and consultancy fees from Roche and speaker fees from Roche, AstraZeneca, Eisai and Chugai, FH received travel support from Bayer, AbbVie and Gilead. LDT has nothing to report. MBe has nothing to report. LR received consulting fees from AbbVie, AstraZeneca, Basilea, Bayer, BMS, Eisai, Elevar Therapeutics, Exelixis, Genenta, Hengrui, Incyte, Ipsen, IQVIA, Jazz Pharmaceuticals, MSD, Nerviano Medical Sciences, Roche, Servier, Taiho Oncology, Zymeworks; lecture fees from AstraZeneca, Bayer, BMS, Guerbet, Incyte, Ipsen, Roche, Servier; travel expenses from AstraZeneca; and institutional research funding from Agios, AstraZeneca, BeiGene, Eisai, Exelixis, Fibrogen, Incyte, Ipsen, Lilly, MSD, Nerviano Medical Sciences, Roche, Servier, Taiho Oncology, TransThera Sciences, Zymeworks. BM has nothing to declare. MTr has received research grants from Albireo, Alnylam, Cymabay, Falk, Genentech, Gilead, Intercept, MSD, Takeda and Ultragenyx and travel grants from AbbVie, Falk, Gilead, Intercept and Janssen, He further has advised for AbbVie, Agomab, Albireo, BiomX, Boehringer Ingelheim, Chemomab Falk Pharma GmbH, Genfit, Gilead, Hightide, Intercept, Ipsen, Janssen, Mirum, MSD, Novartis, Phenex, Pliant, Rectify, Regulus, Siemens and Shire and has served as speaker for Albireo, BMS, Boehringer Ingelheim, Falk, Gilead, Intercept, Ipsen, Madrigal and MSD. He is a coinventor of patents for the medical use of norUDCA (nor-ursodeoxycholic acid/norucholic acid) filed by the Medical Universities of Graz and Vienna. CL has nothing to report. RS is an investigator for Bayer, BMS and Roche; he is a consultant for AstraZeneca, Bayer, BMS, Eisai, Ipsen, Lilly and Roche; he received travel support from Bayer and Roche. MP-R is an advisor/consultant for AstraZeneca, Bayer, BMS, Eisai, Ipsen, Lilly, MSD and Roche; he served as a speaker for Bayer, Eisai, Ipsen, Lilly and Roche; he is an investigator for Bayer, BMS, Eisai, Exelixis, Lilly and Roche. MP is an investigator for Bayer, BMS, Eisai, Ipsen, Lilly and Roche; he received speaker honoraria from Bayer, BMS, Eisai, Lilly, MSD and Roche; he is a consultant for Bayer, BMS, Eisai, Ipsen, Lilly, MSD and Roche; he received travel support from Bayer, BMS and Roche. HJC has a consulting or advisory role at Roche, Eisai, Bayer, ONO, BMS, MSD, Sanofi, Servier, AstraZeneca, Sillajen and has received research grants from Roche, Dong-A ST, Boryung Pharmaceuticals, HK inno.N and Hanmi Pharm. MRak received lecture fees from AstraZeneca. DJP received lecture fees from ViiV Healthcare, Bayer Healthcare, BMS, Roche, Eisai, Falk Foundation, travel expenses from BMS and Bayer Healthcare: consulting fees for Mina Therapeutics, EISAI, Roche, DaVolterra, Mursla, Exact Sciences and AstraZeneca; research funding (to institution) from MSD and BMS.

### Patient consent for publication Not applicable.

**Ethics approval** This study involves human participants. This retrospective analysis was approved by the local ethics committees of Imperial College London (17/YH/0015) as well as the Medical University of Vienna (EK 2033/2017). Participants gave informed consent to participate in the study before taking part.

Provenance and peer review Not commissioned; externally peer reviewed.

**Data availability statement** Data are available on reasonable request. Data will be made available on reasonable request from the corresponding authors.

Supplemental material This content has been supplied by the author(s). It has not been vetted by BMJ Publishing Group Limited (BMJ) and may not have been peer-reviewed. Any opinions or recommendations discussed are solely those of the author(s) and are not endorsed by BMJ. BMJ disclaims all liability and responsibility arising from any reliance placed on the content. Where the content includes any translated material, BMJ does not warrant the accuracy and reliability of the translations (including but not limited to local regulations, clinical guidelines, terminology, drug names and drug dosages), and is not responsible for any error and/or omissions arising from translation and adaptation or otherwise.

**Open access** This is an open access article distributed in accordance with the Creative Commons Attribution Non Commercial (CC BY-NC 4.0) license, which permits others to distribute, remix, adapt, build upon this work non-commercially, and license their derivative works on different terms, provided the original work is properly cited, appropriate credit is given, any changes made indicated, and the use is non-commercial. See http://creativecommons.org/licenses/by-nc/4.0/.

### ORCID IDS

Antonio D'Alessio http://orcid.org/0000-0002-9164-3671 Oleksandr Petrenko http://orcid.org/0000-0002-8586-4910 Matthias Pinter http://orcid.org/0000-0002-7260-532X Mehrdad Rakaee http://orcid.org/0000-0002-9080-0153 David J Pinato http://orcid.org/0000-0002-3529-0103

### **REFERENCES**

- 1 Finn RS, Qin S, Ikeda M, et al. Atezolizumab plus Bevacizumab in Unresectable Hepatocellular Carcinoma. N Engl J Med 2020:382:1894–905.
- 2 Abou-Alfa GK, Lau G, Kudo M, et al. Tremelimumab plus Durvalumab in Unresectable Hepatocellular Carcinoma. NEJM Evid 2022;1:EVIDoa2100070.
- Llovet JM, Montal R, Sia D, et al. Molecular therapies and precision medicine for hepatocellular carcinoma. Nat Rev Clin Oncol 2018;15:599–616.
- 4 Scheiner B, Pomej K, Kirstein MM, et al. Prognosis of patients with hepatocellular carcinoma treated with immunotherapy development and validation of the CRAFITY score. J Hepatol 2022;76:353–63.
- 5 Greten TF, Villanueva A, Korangy F, et al. Biomarkers for immunotherapy of hepatocellular carcinoma. Nat Rev Clin Oncol 2023;20:780–98.
- 6 Zhu AX, Abbas AR, de Galarreta MR, et al. Molecular correlates of clinical response and resistance to atezolizumab in combination with bevacizumab in advanced hepatocellular carcinoma. Nat Med 2022:28:1599–611.
- 7 Sahu A, Kose K, Kraehenbuehl L, et al. In vivo tumor immune microenvironment phenotypes correlate with inflammation and vasculature to predict immunotherapy response. Nat Commun 2022:13:5312.
- 8 Reck M, Rodríguez-Abreu D, Robinson AG, et al. Pembrolizumab versus Chemotherapy for PD-L1-Positive Non-Small-Cell Lung Cancer. N Engl J Med 2016;375:1823–33.
- 9 Xue R, Zhang Q, Cao Q, et al. Liver tumour immune microenvironment subtypes and neutrophil heterogeneity. Nature New Biol 2022;612:141–7.
- 10 Pfister D, Núñez NG, Pinyol R, et al. NASH limits anti-tumour surveillance in immunotherapy-treated HCC. Nature New Biol 2021:592:450–6.
- 11 Sia D, Jiao Y, Martinez-Quetglas I, et al. Identification of an Immunespecific Class of Hepatocellular Carcinoma, Based on Molecular Features. Gastroenterology 2017;153:812–26.
- Montironi C, Castet F, Haber PK, et al. Inflamed and non-inflamed classes of HCC: a revised immunogenomic classification. Gut 2023:72:129–40.
- 13 Väyrynen JP, Lau MC, Haruki K, et al. Prognostic Significance of Immune Cell Populations Identified by Machine Learning in Colorectal Cancer Using Routine Hematoxylin and Eosin-Stained Sections. Clin Cancer Res 2020;26:4326–38.
- 14 Rakaee M, Adib E, Ricciuti B, et al. Association of Machine Learning– Based Assessment of Tumor-Infiltrating Lymphocytes on Standard Histologic Images With Outcomes of Immunotherapy in Patients With NSCLC. JAMA Oncol 2023:9:51.
- 15 Bankhead P, Loughrey MB, Fernández JA, et al. QuPath: Open source software for digital pathology image analysis. Sci Rep 2017;7:16878.
- 16 Hothorn T, Lausen B. On the exact distribution of maximally selected rank statistics. Comput Stat Data Anal 2003;43:121–37.
- 17 Lin H, Kryczek I, Li Ś, et al. Stanniocalcin 1 is a phagocytosis checkpoint driving tumor immune resistance. Cancer Cell 2021;39:480–93.
- 18 Sun Q, Hong Z, Zhang C, et al. Immune checkpoint therapy for solid tumours: clinical dilemmas and future trends. Signal Transduct Target Ther 2023;8:320.
- 19 Delgado A, Guddati AK. Clinical endpoints in oncology a primer. Am J Cancer Res 2021;11:1121–31.
- 20 Sangro B, Chan SL, Kelley RK, et al. Four-year overall survival update from the phase III HIMALAYA study of tremelimumab plus durvalumab in unresectable hepatocellular carcinoma. Ann Oncol 2024;35:448–57.
- 21 Li SQ, Yang Y, Ye LS. Angiogenesis and immune checkpoint dual blockade: Opportunities and challenges for hepatocellular carcinoma therapy. World J Gastroenterol 2022;28:6034–44.
- 22 Salgado R, Denkert C, Demaria S, et al. The evaluation of tumorinfiltrating lymphocytes (TILs) in breast cancer: recommendations by an International TILs Working Group 2014. Ann Oncol 2015;26:259–71.



- 23 Chen B, Pan Y, Xu X, et al. Inhibition of EPS8L3 suppresses liver cancer progression and enhances efficacy of sorafenib treatment. Biomedicine & Pharmacotherapy 2020;128:110284.
- 24 Zeng Q, Klein C, Caruso S, et al. Artificial intelligence-based pathology as a biomarker of sensitivity to atezolizumab-bevacizumab in patients with hepatocellular carcinoma: a multicentre retrospective study. *Lancet Oncol* 2023;24:1411–22.
- 25 Bang YH, Lee C-K, Bang K, et al. Artificial Intelligence-Powered Spatial Analysis of Tumor-Infiltrating Lymphocytes as a Potential Biomarker for Immune Checkpoint Inhibitors in Patients with Biliary Tract Cancer. Clin Cancer Res 2024;30:4635–43.
- 26 Zheng L, Qin S, Si W, et al. Pan-cancer single-cell landscape of tumor-infiltrating T cells. Science 2021;374:abe6474.